

EMU Detection of a Large and Low Surface Brightness Galactic SNR G288.8–6.3

MIROSLAV D. FILIPOVIĆ ¹, SHI DAI ¹, BOJAN ARBUTINA ², NATASHA HURLEY-WALKER ³, ROBERT BROSE ⁴,
WERNER BECKER ^{5,6}, HIDETOSHI SANO ⁷, DEJAN UROŠEVIĆ ², T.H. JARRETT ^{8,1}, ANDREW M. HOPKINS ⁹,
RAMI Z. E. ALSABERI ¹, R. ALSULAMI ¹⁰, CRISTOBAL BORDIU ¹¹, BRIANNA BALL ¹², FILOMENA BUFANO ¹¹,
CHRISTOPHER BURGER-SCHIEDLIN ^{4,13}, EVAN CRAWFORD ¹, JAYANNE ENGLISH ¹⁴, FRANK HABERL ⁵,
ADRIANO INGALLINERA ¹¹, ANNA D. KAPINSKA ¹⁵, PATRICK J. KAVANAGH ¹⁶, BÄRBEL S. KORIBALSKI ^{17,1},
ROLAND KOTHES ¹², SANJA LAZAREVIĆ ^{1,18}, JONATHAN MACKEY ^{4,19}, GAVIN ROWELL ¹⁰, DENIS LEAHY ²⁰,
SARA LORU ¹¹, PETER J. MACGREGOR ^{1,17}, LUCIANO NICASTRO ²¹, RAY P. NORRIS ^{1,17}, SIMONE RIGGI ¹¹,
MANAMI SASAKI ²², MILORAD STUPAR ¹, CORRADO TRIGILIO ¹¹, GRAZIA UMANA ¹¹, TESSA VERNSTROM ²³ AND
BRANISLAV VUKOTIĆ ¹⁸

¹Western Sydney University, Locked Bag 1797, Penrith South DC, NSW 2751, Australia

²Department of Astronomy, Faculty of Mathematics, University of Belgrade, Studentski trg 16, 11000 Belgrade, Serbia

³International Centre for Radio Astronomy Research, Curtin University, Bentley, WA 6102, Australia

⁴Dublin Institute for Advanced Studies, Astronomy & Astrophysics Section, DIAS Dunsink Observatory, Dublin, D15 XR2R, Ireland

⁵Max-Planck-Institut für extraterrestrische Physik, Gießenbachstraße 1, D-85748 Garching, Germany

⁶Max-Planck-Institut für Radioastronomie, Auf dem Hügel 69, 53121 Bonn, Germany

⁷Faculty of Engineering, Gifu University, 1-1 Yanagido, Gifu 501-1193, Japan

⁸Department of Astronomy, University of Cape Town, Private Bag X3, Rondebosch 7701, South Africa

⁹School of Mathematical and Physical Sciences, 12 Wally's Walk, Macquarie University, NSW 2109, Australia

¹⁰School of Physical Sciences, The University of Adelaide, Adelaide 5005, Australia

¹¹INAF – Osservatorio Astrofisico di Catania, via Santa Sofia 78, I-95123 Catania, Italia

¹²Dominion Radio Astrophysical Observatory, Herzberg Astronomy and Astrophysics, National Research Council Canada, PO Box 248, Penticton BC V2A 6J9, Canada

¹³School of Physics, University College Dublin, Belfield, Dublin, D04 V1W8, Ireland

¹⁴Department of Physics and Astronomy, University of Manitoba, Winnipeg, Manitoba R3T 2N2, Canada

¹⁵National Radio Astronomy Observatory, PO Box 0, Socorro, NM87801, USA

¹⁶Department of Experimental Physics, Maynooth University, Maynooth, Co. Kildare, Ireland

¹⁷CSIRO Space and Astronomy, Australia Telescope National Facility, PO Box 76, Epping, NSW 1710, Australia

¹⁸Astronomical Observatory, Volgina 7, 11060 Belgrade, Serbia

¹⁹School of Physics, University College Dublin, Belfield, Dublin 4, Ireland

²⁰Department of Physics and Astronomy, University of Calgary, Calgary, Alberta, T2N 1N4, Canada

²¹INAF – Osservatorio di Astrofisica e Scienza dello Spazio di Bologna, Via Piero Gobetti 93/3, I-40129 Bologna, Italy

²²Dr Karl Remeis Observatory, Erlangen Centre for Astroparticle Physics, Friedrich-Alexander-Universität Erlangen-Nürnberg, Sternwartstraße 7, 96049 Bamberg, Germany

²³ICRAR, The University of Western Australia, 35 Stirling Hw, 6009 Crawley, Australia

ABSTRACT

We present the serendipitous detection of a new Galactic Supernova Remnant (SNR), G288.8–6.3, using data from the Australian Square Kilometre Array Pathfinder (ASKAP)-Evolutionary Map of the Universe (EMU) survey. Using multi-frequency analysis, we confirm this object as an evolved Galactic SNR at high Galactic latitude with low radio surface brightness and typical SNR spectral index of $\alpha = -0.41 \pm 0.12$. To determine the magnetic field strength in SNR G288.8–6.3, we present the first derivation of the equipartition formulae for SNRs with spectral indices $\alpha > -0.5$. The angular size is $1^{\circ}8 \times 1^{\circ}6$ ($107.6' \times 98.4'$) and we estimate that its intrinsic size is ~ 40 pc which implies a distance of ~ 1.3 kpc and a position of ~ 140 pc above the Galactic plane. This is one of the largest angular size

and closest Galactic SNRs. Given its low radio surface brightness, we suggest that it is about 13 000 years old.

1. INTRODUCTION

The census of the Galactic SNR population is well understood to be under-represented (Foster et al. 2013; Dokara et al. 2021; Ball et al. 2023). Only ~ 300 such objects are confirmed (Green 2022; Ferrand & Safi-Harb 2012) with expectations that up to an almost order of magnitude more could exist in the Milky Way (Ranasinghe & Leahy 2022). Most of the missing Galactic SNRs are expected to be low-surface brightness or in complex regions where clear distinctions from other source types (e.g. HII regions) are challenging. At the same time, new, bright, small size (compact) and presumably young SNRs are not likely to be found in abundance (Ranasinghe et al. 2021).

With their improved capabilities and low surface-brightness sensitivity, the latest generation of radio telescopes, including ASKAP, MeerKAT, Murchison Widefield Array (MWA) and Low-Frequency Array (LOFAR), are expected to discover many of these missing Galactic SNRs. Indeed, several recent discoveries such as the intergalactic SNR J0624–6948 (Filipović et al. 2022a), the Galactic SNRs G181.1–9.5 (Kothes et al. 2017), Hoinga (Becker et al. 2021), G118.4+37.0 (Calvera; Arias et al. 2022), J1818.0–1607 (Ibrahim et al. 2023) and G121.1–1.9 (Khabibullin et al. 2023) confirm this expectation. These SNRs are mainly located well outside the Galactic Plane where they can preserve their typical circular SNR shape for longer timeframes, in the presumably low-density environment while also becoming lower surface-brightness as compared to typical SNRs.

The majority of known SNRs were discovered in radio surveys with mature instruments, such as the Very Large Array (VLA), Parkes, the Australia Telescope Compact Array (ATCA), Effelsberg, Molonglo Observatory Synthesis Telescope (MOST), and the synthesis telescope at the Dominion Radio Astrophysical Observatory (DRAO ST) as part of the Canadian Galactic Plane Survey (CGPS, Taylor et al. 2003). In addition to established SNRs, many candidates have also been identified and await confirmation. For example, Duncan et al. (1997) and Stupar et al. (2007, 2008) revealed several filamentary and low-surface brightness nebulosities from the Parkes-MIT-NRAO (PMN) survey (Wright et al. 1994) and the AAO/UKST H α survey as possible candidate SNRs. Here we report the detection of a new Galactic SNR which could be a representative of the missing Galactic SNR population.

In Section 2, we first derive the equipartition formulae for determining magnetic fields in SNRs with spectral indices $\alpha > -0.5$, which will be applied to SNR G288.8–6.3. Observations and data analysis are described in Section 3. We present and discuss our results in Section 4. Finally, the conclusions are given in Section 5.

2. ADAPTED EQUIPARTITION CALCULATION FOR $\alpha > -0.5$

The diffusive shock acceleration (DSA) theory in the test-particle regime predicts that for strong shocks (with compression ~ 4) the particle spectrum will be a power-law with energy index $\Gamma = 2$ (Bell 1978), which leads to the radio spectral index $\alpha = -\frac{\Gamma-1}{2} = -0.5$. Observed SNRs indeed have an average spectral index ~ -0.5 (Reynolds et al. 2012; Galvin & Filipovic 2014; Bozzetto et al. 2017; Maggi et al. 2019; Filipović & Tothill 2021), but there are remnants with $\alpha > -0.5$, which may also be the case with G288.8–6.3, as we shall see in the Subsection 4.1.

Energy indices $\Gamma < 2$ can not be explained by the test-particle DSA, but assuming that the energy index is not directly related to shock compression, we can still try to estimate the magnetic field strength for such remnants through an adapted equipartition calculation. The synchrotron flux density can be written as (Arbutina 2017)

$$S_\nu = \frac{4\pi}{3} f \theta^3 d c_5 K_e (B \sin \Theta)^{(\Gamma+1)/2} \left(\frac{\nu}{2c_1} \right)^{(1-\Gamma)/2}, \quad (1)$$

where c_1 and c_5 are defined in Pacholczyk (1970), B is the magnetic field strength, Θ the pitch angle, K_e the constant in the power-law energy distributions of cosmic ray (CR) electrons $N(E) = K_e E^{-\Gamma}$, ν is the frequency, f is the volume filling factor, θ the angular radius and d is the distance. We shall use averaged sine of the pitch angle, $\frac{\sqrt{\pi}}{2} \frac{\Gamma(\frac{\Gamma+5}{4})}{\Gamma(\frac{\Gamma+7}{4})}$. From the above equation, using spectral index $\alpha = -\frac{\Gamma-1}{2}$ we can write

$$K_e B^{\alpha+1} = J, \quad (2)$$

where J is a function that can be calculated from observable quantities. To estimate B , we need to know some relation between K_e and B , which is the basis for the minimum-energy or equipartition calculation (Pacholczyk 1970). In SNRs, the equipartition between CRs energy and magnetic field energy does not seem to be reached. Still, the magnetic field energy density may be comparable to the energy density of CR electrons (Urošević et al. 2018).

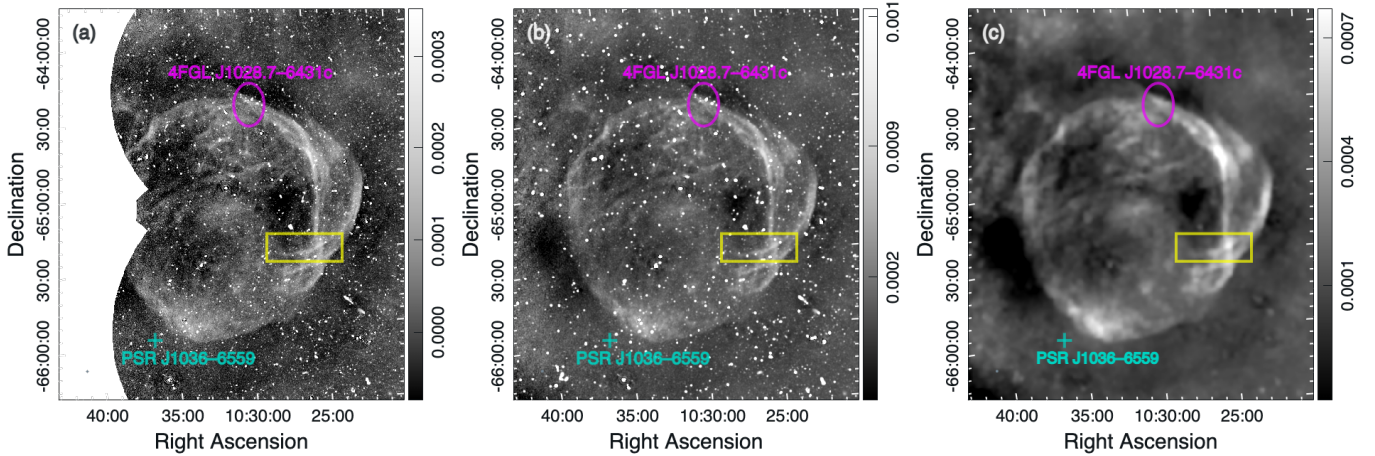


Figure 1. ASKAP image of the Galactic SNR G288.8–6.3 at 943 MHz. On the left (a) is the publicly released image with a synthesised beam of $15'' \times 15''$ while in the middle (b) we show an extended and re-processed image that is convolved to the resolution of $30'' \times 30''$. On the right in the image (c), to enhance the diffuse emission we show image (b) that is scaled with a $90''$ box using the multi-resolution filtering method of Rudnick (2002). The magenta ellipse marks the position of gamma-ray source 4FGL J1028.7–6431c (68% containment), while the cyan cross marks the position of nearby radio pulsar J1036–6559. The yellow rectangular box marks the area covered in Figure 5. The grey scale (in Jy beam^{-1}) is displayed on the right side, with the (a) and (b) images using a logarithmic scale and the (c) image using a linear scale.

CR energy density for a power-law particle distribution of electrons $f(p) = kp^{-\Gamma-2}$ (Arbutina et al. 2012, 2013; Arbutina 2017) can be written as

$$\begin{aligned} \epsilon_{\text{CR}} &= \int_{p_{\text{inj}}}^{p_{\infty}} 4\pi kp^{-\Gamma} (\sqrt{p^2 c^2 + m_e^2 c^4} - m_e c^2) dp \\ &= 4\pi kc(m_e c)^{2-\Gamma} \int_{\frac{p_{\text{inj}}}{m_e c}}^{\frac{p_{\infty}}{m_e c}} x^{-\Gamma} (\sqrt{x^2 + 1} - 1) dx, \quad x = \frac{p}{m_e c} \\ &= K_e (m_e c^2)^{2-\Gamma} I_1, \end{aligned}$$

where $K_e = 4\pi kc^{\Gamma-1}$. Injection momentum can be written as $p_{\text{inj}} = \xi p_{\text{th}} = \xi \sqrt{2m_e k T_e}$, where ξ is injection parameter related to the injection efficiency (Blasi et al. 2005)

$$\eta = \frac{4}{\sqrt{\pi}} \frac{1}{\Gamma - 1} \xi^3 e^{-\xi^2}. \quad (4)$$

For T_e , we can provisionally assume $T_e \sim 0.4T_p$ (for $v_s \sim 600 \text{ km s}^{-1}$ Ghavamian et al. 2013), where T_p can be calculated from Rankine-Hugoniot jump conditions.

Assuming synchrotron losses, the maximum electron energy (Zirakashvili & Aharonian 2007) is

$$E_{\infty} = p_{\infty} c = \frac{1}{1 + \sqrt{\kappa}} \frac{\sigma - 1}{3\sigma} \frac{m_e^2 c^3 v_s}{\sqrt{\frac{2}{27} e^3 B}}, \quad (5)$$

where σ shock compression, $\kappa = B_0/B = 1/\sqrt{(1 + 2\sigma^2)/3}$, B_0 ambient magnetic field. If $\epsilon_{\text{CR}} \approx \epsilon_B = \frac{1}{8\pi} B^2$ then

$$K_e = \frac{(m_e c)^{\Gamma-2}}{8\pi I_1} B^2, \quad (6)$$

and the magnetic field estimate is

$$B^{\alpha+3} = 8\pi (m_e c)^{2-\Gamma} I_1 J. \quad (7)$$

If we had used proton equipartition, then

$$K_p = \frac{(m_p c)^{\Gamma-2}}{8\pi I_1} B^2, \quad (8)$$

and with $p_{\text{inj}} = \xi \sqrt{2m_p k T_p}$, $E_{\infty} = \frac{3}{8} \frac{v_s}{c} e B R$ and $K_{ep} = \left(\frac{m_e T_e}{m_p T_p}\right)^{\alpha}$ (Arbutina & Zeković 2021), the magnetic field would be

$$B^{\alpha+3} = 8\pi (m_p c)^{2-\Gamma} I_1 J / K_{ep}. \quad (9)$$

In Subsection 4.1 we will apply Eqs. (7) and (9) to estimate magnetic field strength in G288.8–6.3.

3. OBSERVATIONS AND DATA

As a part of the large scale ASKAP-EMU project (AS201), this part of the radio sky was observed in January 2023 with a complete set of 36 ASKAP antennas at the central frequency of 943.4 MHz and bandwidth of 288 MHz. All data can be found in the CSIRO ASKAP Science Data Archive (CASDA¹). The observations containing this object are the tile EMU_1003–64 corresponding to ASKAP scheduling block SB46974. The data were processed using the ASKAPsoft pipeline, including multi-frequency synthesis imaging, multi-scale clean and self-calibration (Guzman et al. 2019). The

¹ <https://research.csiro.au/casda>

resulting 943 MHz EMU image has a sensitivity of $\sigma=25 \mu\text{Jy beam}^{-1}$ and a synthesised beam of $15'' \times 15''$ (Figure 1a).

A small portion of the eastern side of G288.8–6.3 is at the edge of the EMU observing block (tile) (see Figure 1a). The EMU project is surveying the full southern sky, enabling this serendipitous detection of G288.8–6.3. Currently, only Stokes I and V images are available.

In order to extend the view further towards the east, we re-imaged G288.8–6.3 to a lower primary beam cutoff. We used visibilities for beams 5, 10, 11, 16, 17, 22, 23 and 29 of SB46974 and re-imaged with the same continuum settings of the above described ASKAP pipeline (Figure 1b). The beams were then convolved to a common circular beam of $30'' \times 30''$ and mosaiced together using the holography beams from the SB metadata. We use a lower weight cutoff of 0.01, instead of the default 0.20 to extend the coverage of the mosaic to the east. This cutoff may introduce errors as the holography measurements only just sample the primary field of view (Hotan 2016), and may not fully characterise the edge beams imaged here. We measured the image Root Mean Squared (rms) of $\sigma=31 \mu\text{Jy beam}^{-1}$.

Finally, we used the multiresolution filtering method of Rudnick (2002) to enhance the diffuse emission of G288.8–6.3 as seen in Figure 1c.

We examined several large-area radio surveys to search for G288.8–6.3 signatures and to derive the flux density as a function of frequency. Only surveys with sensitivity to scales at least that of its diameter ($1.7''$) can be used so that it is not resolved out. At the lowest frequency, we used data taken by the MWA (Tingay et al. 2013; Wayth et al. 2018) for the GaLactic and All-sky MWA (GLEAM; Wayth et al. 2015) survey, at the edge of the 170–231 MHz source-finding mosaics generated by Hurley-Walker et al. (2017) (see Figure 2a).

At 1400 MHz, we used the continuum map of the HI Parkes All-Sky Survey (CHIPASS²; Calabretta et al. 2014), a radio sky survey covering $\text{Dec} < +25^\circ$ at $14.4''$ resolution (see Figure 2b). At 2300 MHz, we used the S-Band Polarization All Sky Survey (S-PASS; Carretti et al. 2019), a 2300-MHz survey of polarised radio emission covering the southern sky ($\text{Dec} < -1^\circ$) at $8.9''$ resolution (see Figure 2c).

To remove the contaminating point sources from the data, we followed the methods previously detailed by Becker et al. (2021) and Araya et al. (2022). We performed source-finding on the MWA and EMU im-

ages, using AEGEAN³ (Hancock et al. 2012, 2018) and its companion tool the Background and Noise Estimator (BANE). We subtracted the MWA 200-MHz point sources from the image using a further ancillary tool AERES. For CHIPASS and S-PASS, we scaled the flux densities of the sources detected in the EMU image by a spectral index (defined by $S \propto \nu^\alpha$, where S is flux density, ν is the frequency and α is the spectral index) reasonable at these flux densities ($\alpha = -0.83$), convolved the model to their lower resolutions and performed subtraction.

Finally, we used several other large-area sky surveys such as PMN survey (Section 4.1), HI4PI (Section 4.3), SuperCOSMOS (Section 4.2), Wide-Field Infrared Survey Explorer (WISE) (Section 4.4), extended Röntgen Survey with an Imaging Telescope Array (eROSITA) All Sky Survey (eRASS; Section 4.5) and Fermi (Section 4.6).

4. RESULTS AND DISCUSSION

We have serendipitously found a large-scale object in our new ASKAP-EMU survey (Norris et al. 2021) which we classify as the new Galactic SNR G288.8–6.3 (Figure 1). Our detection and classification of this Galactic SNR is primarily based on the object morphology, size and multi-frequency appearance of G288.8–6.3 and the method is described in Hurley-Walker et al. (2019a, Section 2.4), Filipović et al. (2022a) and Bozzetto et al. (2023). We note that Duncan et al. (1997) and Stupar et al. (2008) identified this object as a possible SNR candidate but wrongly named G288.7–6.3 because they couldn't define G288.8–6.3 exact central position and extent.

4.1. SNR G288.8–6.3 Radio-continuum Properties

We used the Minkowski tensor analysis tool BANANA⁴ (Collischon et al. 2021) to determine the centre of G288.8–6.3 to be at $\text{RA}(\text{J2000}) = 10^{\text{h}}30^{\text{m}}22^{\text{s}}.3$ and $\text{Dec}(\text{J2000}) = -65^\circ 12' 46''.5$, with a size of 1.8×1.6 (107.6×98.4) at a position angle of 30° .

To remove gradients from the large-scale Galactic diffuse emission in MWA, CHIPASS and S-PASS images, we fit a 2-D plane to the region around G288.8–6.3 using POLYGON-FLUX⁵ (Hurley-Walker et al. 2019a). The source-subtracted, backgrounded data are shown in Figure 2. This tool was also used to obtain total radio flux densities at these three frequencies (200, 1400 and 2300 MHz) which produced a spectral index of

² <https://www.atnf.csiro.au/people/mcalabre/CHIPASS/index.html>

³ <https://github.com/PaulHancock/Aegean>

⁴ <https://github.com/ccollischon/banana>

⁵ <https://github.com/nhurleywalker/polygon-flux>

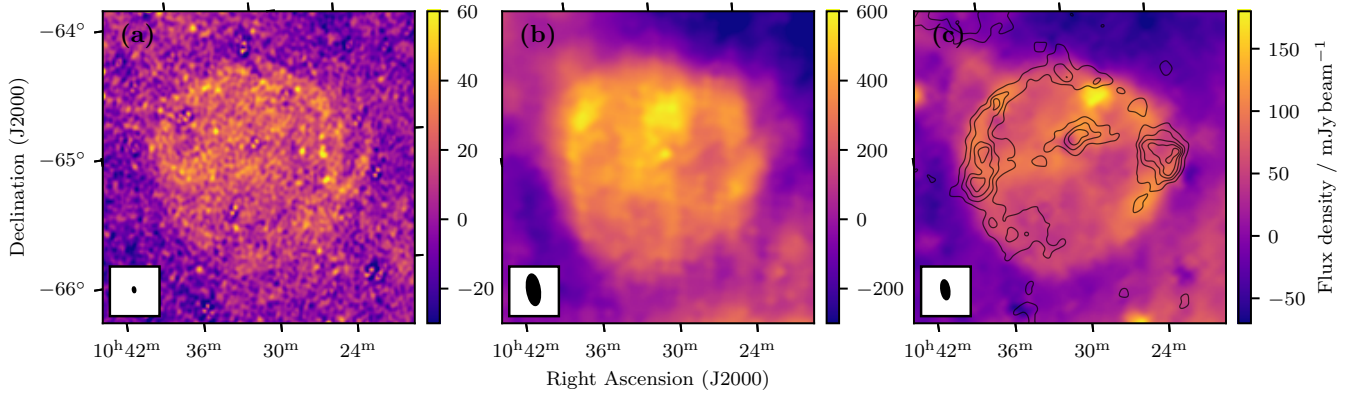


Figure 2. 2.5×2.5 region surrounding G288.8–6.3 at MWA 200 MHz (a), CHIPASS 1400 MHz (b), and S-PASS 2300 MHz (c) after source and background subtraction as described in Section 4.1. The contours on the third panel show the total linear polarisation measured in S-PASS, in steps of $4 \times$ the local RMS noise, $38 \mu\text{Jy beam}^{-1}$. The full-width-half-maximum of the point spread function is shown as a solid black ellipse in the lower left of each panel.

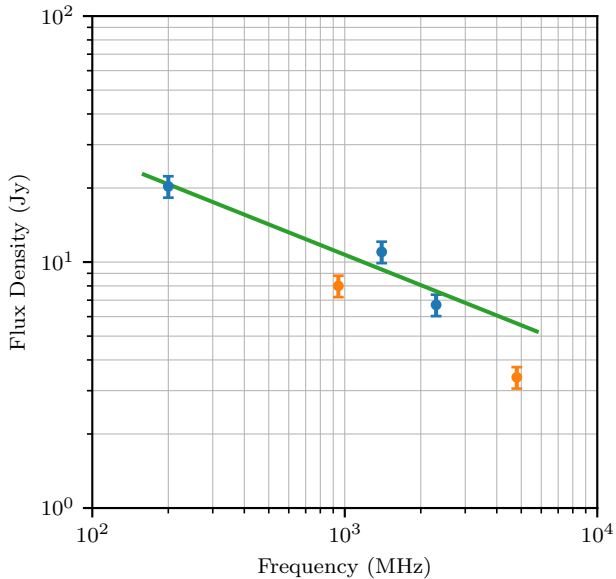


Figure 3. Radio flux densities as a function of frequency. A power-law fit based on flux density measurements (blue points) from MWA, CHIPASS and S-PASS surveys with $S_{1\text{GHz}} = 10.92 \pm 0.06 \text{ Jy}$ and $\alpha = -0.41 \pm 0.12$ is shown with a green line. Two orange points are flux density measurements from ASKAP and PMN surveys and they are not included in the spectral index estimate.

$\alpha = -0.41 \pm 0.12$. Errors were assigned as 20, 10 and 10% respectively. The data and a power-law fit are shown in Figure 3.

SNR G288.8–6.3 is also detected in the PMN survey at 4850 MHz, although the median filter applied to the data makes it impossible to obtain reliable flux densities for large objects. After a similar subtraction of point sources, we estimate lower flux density limits of $S_{\text{PMN}} = 3.4 \text{ Jy}$ and $S_{\text{ASKAP}} = 8.0 \text{ Jy}$. This indicates a

missing flux density of $> 50\%$ at both frequencies and we did not use these two values for the spectral index estimate. Even if we included these two flux density estimates, the spectral index would be only fractionally steeper ($\alpha = -0.51 \pm 0.12$) but still within the range of the above estimate of $\alpha = -0.41 \pm 0.12$.

This spectral index of $\alpha = -0.41 \pm 0.12$ is somewhat flatter than that of average shell type SNRs but within the observed range of -0.55 ± 0.20 for the Galaxy and range of nearby galaxy SNRs (Reynolds et al. 2012; Galvin & Filipovic 2014; Bozzetto et al. 2017; Maggi et al. 2019; Filipović & Tothill 2021). We also note an enhanced extended radio emission in the centre of G288.8–6.3 which could indicate the presence of a Pulsar Wind Nebulae (PWN). However, we couldn’t independently confirm this emission’s nature as it could also come from the G288.8–6.3 shell.

S-PASS also enables an examination of the polarisation features; the shell of G288.8–6.3 shows up clearly in total linear polarisation with absolute intensities of $\sim 600 \mu\text{Jy beam}^{-1}$ and fractionally about 1% (contours in panel (c) of Figure 2). An extended feature of similar brightness north of the shell centre may be a polarised filament viewed in projection or potentially confusion from the surrounding point sources. Future polarisation measurements with Polarization Sky Survey of the Universe’s Magnetism (POSSUM; Gaensler et al. 2010) will enable better measurement of the G288.8–6.3 polarisation features.

Most SNRs are characterised by their position in the brightness-to-diameter (Σ -D) parameter space. Based on the above-measured flux densities and the angular size of G288.8–6.3, we estimate a radio surface brightness at 1 GHz of $\Sigma = 1.4 \times 10^{-22} \text{ W m}^{-2} \text{ Hz}^{-1} \text{ sr}^{-1}$ (assuming the emission to be spread smoothly over the SNR

boundaries defined above). This value places G288.8–6.3 in the bottom area of the SNR $\Sigma - D$ diagram

(for a sample of 110 known Galactic SNRs used as calibrators, see Vukotić et al. 2019) and indicates an intrinsic diameter of 40 pc (± 9 pc), determined by the analysis of the probability density function in the $\Sigma - D$ plane and the corresponding orthogonal fitting procedure (Vukotić et al. 2019). Coupled with the above measured angular size, this indicates a 1.3 kpc (± 0.4 kpc) distance which is among the 10 closest Galactic SNRs. Given this distance range and the Galactic latitude of $-6^\circ.3$, G288.8–6.3 is 140 pc away from the Galactic plane, suggesting that it is still inside the thin disk.

The intrinsic size of ~ 40 pc is close to the median size of all known SNRs in our Galaxy (Green 2022). At one end, the largest would be the Monoceros loop (G205.5+0.5) with a diameter of ~ 128 pc (Zhao et al. 2020). At the other end, the smallest would be ~ 140 year young SNR G1.9+0.3 with a diameter of only 3.9 pc (Luken et al. 2020). A similar range of SNR diameters can be found in the Large Magellanic Cloud (LMC) (Bozzetto et al. 2017; Yew et al. 2021; Bozzetto et al. 2023) where SNR MCSNR 0450–70 is the largest ($102 \times 75 \pm 1$ pc) (Cajko et al. 2009) and SN1987A would be the smallest. There are only ~ 12 known Galactic SNRs with a larger angular size listed in the catalogue of Green (2022). The most similar (in angular size) are Galactic SNRs G89.0+4.7 (HB21) (Gao et al. 2011) and G7.5–1.7 (Hurley-Walker et al. 2019b,a) but both of these SNRs are much brighter radio sources.

G288.8–6.3 has somewhat lower surface brightness (Figure 4) than the majority of known Magellanic Clouds and Galactic SNRs with established distance (Vukotić et al. 2019). Given the low radio surface brightness of G288.8–6.3, we suggest it is in an evolved Sedov stage and about 13 000 years old. Assuming an ambient density of 0.17 cm^{-3} (Misiriotis et al. 2006) and Supernova (SN) energy of $E_0 = 10^{51}$ erg we can estimate the shock velocity to be $v_s \sim 600 \text{ km s}^{-1}$ and the Sedov age about ~ 10 000 years. Taking into account the preceding free expansion phase, a better description of shell dynamics is given by a formula (Finke & Dermer 2012; Bozzetto et al. 2017)

$$\frac{1}{2}v_s^2 = \frac{1}{2} \left(\frac{dR}{dt} \right)^2 = \frac{k_1 E_0}{k_2 M_0 + 4\pi R^3 \rho_0 / 3}, \quad (10)$$

where constant k_1 is determined so that the evolution of a shell for large radii R tend toward Sedov’s solution, while k_2 is obtained from initial conditions. For a rough estimate of SN ejecta mass $M_0 \sim 5 M_\odot$ and initial velocity $v_0 = \sqrt{\frac{2k_1 E_0}{k_2 M_0}} \approx 5000 \text{ km s}^{-1}$, by integrating the last equation we get an age estimate of 13 000 years. Since

the estimates of the ambient density range from 0.11 to 0.24 cm^{-3} (Wolfire et al. 2003) for an assumed distance of 1.3 kpc and $z=140$ pc, this uncertainty in density alone would give an age range ~ 11 000–15 000 years. However, it is difficult to put exact age limits, given the uncertainty in other parameters.

To estimate the magnetic field strength in G288.8–6.3 we use the adapted equipartition calculation described previously. By applying Eq. (7), taking for the filling factor $f = 0.1$, compression $\sigma \approx 4$ and $\xi \approx 4$ (for non-modified strong shocks) and using the observable and calculated quantities of G288.8–6.3 (including the 1 GHz flux density of 10.92 Jy) we find $B = 7.7 \mu\text{G}$ in the ambient field of $2.3 \mu\text{G}$. On the other hand, if we apply Eq. (9), B would be $41.7 \mu\text{G}$ in the ambient field of $12.6 \mu\text{G}$.

At the age of 13 000 years, G288.8–6.3 is among a couple of dozen known historical Galactic SNRs. One could compare its possible intrinsic brightness at the time of explosion to the well-studied SN1054 (Crab nebulae). With the assumption that they are of similar type of SN explosion and relying on Chinese historical reports about the SN1054 brightness (as bright as Venus or $m \sim -4.5$ at a distance of 2 kpc) at the time of the explosion (Filipović et al. 2021a,b, 2022b), we estimate that G288.8–6.3 SN explosion would be $m \sim -5.4$ magnitudes. This would indicate that the G288.8–6.3 explosion was likely to have been seen even during the daytime in the southern hemisphere.

There is no known radio pulsar or any circularly polarised compact object (with $V/I > 0.5\%$) within the borders of G288.8–6.3. Just outside the southeast edge of G288.8–6.3, we find the known pulsar J1036–6559 (Figure 1) with a spin period of 0.5335 s and dispersion measure of $158.36 \text{ cm}^{-3} \text{ pc}$ (Bates et al. 2012). The pulsar has a characteristic age of ~ 6 Myr and a surface magnetic field of $\sim 8 \times 10^{11}$ G, which is typical for normal pulsars (Manchester et al. 2005). According to the YMW16 electron density model (Yao et al. 2017), the distance to PSR J1036–6559 is ~ 2 kpc. If we assume that the two are connected, for PSR J1036–6559 to travel from the centre of G288.8–6.3 to its present position (~ 22 pc; assuming motion to be perpendicular to the line of sight) over the age of 13 000 years it would require a transverse velocity of $\sim 1650 \text{ km s}^{-1}$. This somewhat large velocity for pulsars would leave a prominent trail (the bow-shock; exp. “mouse” (Camilo et al. 2002), DEMS5 (Alsaberi et al. 2019) or “potoroo” (Lazarević et al. in prep.)) that should be observed either in our ASKAP or eROSITA images. Therefore, either SNR G288.8–6.3 is significantly older (> 100 000 years) or much smaller (and closer) than $D=40$ pc (1.3 kpc). It is more plausible

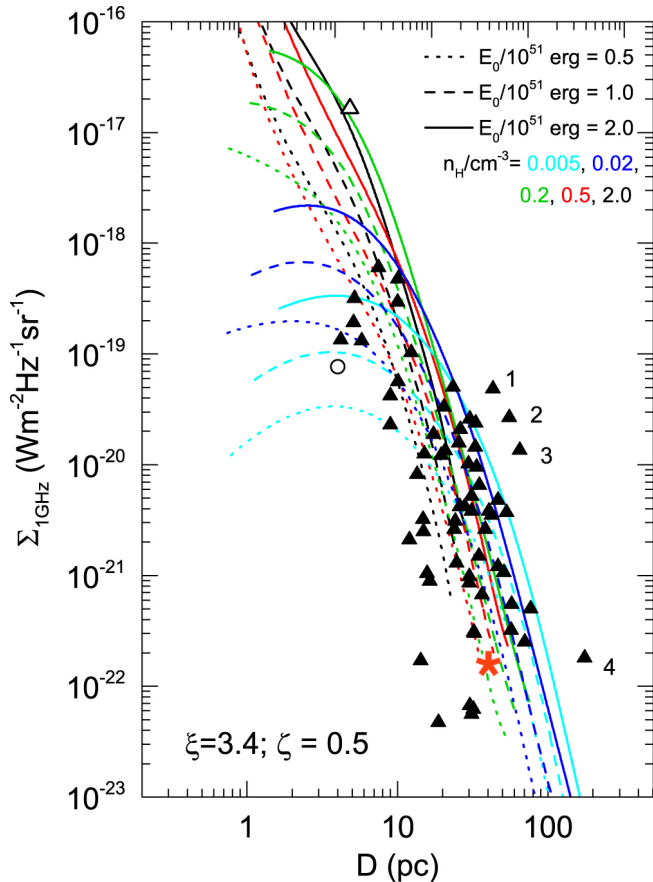


Figure 4. Radio surface brightness-to-diameter diagram for SNRs at a frequency of 1 GHz (black triangles), obtained from numerical simulations (Pavlović et al. 2018, their Fig. 3). Our newly detected SNR G288.8–6.3 is marked with a red star in the bottom right corner while Cassiopeia A is shown with an open triangle. The open circle represents the youngest Galactic SNR, G1.9+0.3 (Luken et al. 2020). Numbers represent the following SNRs: (1) CTB 37A, (2) Kes 97, (3) CTB 37B and (4) G65.1+0.6.

to conclude that there is no direct connection between PSR J1036–6559 and G288.8–6.3.

4.2. G288.8–6.3 H α Emission

Our initial search for signatures at other frequencies showed no signs of emission that could be directly linked to G288.8–6.3 apart from three weak H α emission regions in the AAO/UKST H α SuperCOSMOS⁶ survey (Parker et al. 2005). In Figure 5 we show the H α feature which is marked with yellow arrows in the image. The zoomed frame clearly shows the arc feature overlapping with the radio contours showing likely associations. However, due to numerous point sources such as stars and galaxies in the image field, identifying large-scale

features can be challenging. Stupar et al. (2008, see their Fig. 4) report another H α feature (in the north west rim of G288.8–6.3) with typical SNR optical spectral characteristics and the ratio [S II]/H α of 0.54 that is associated with G288.8–6.3. This further supports that G288.8–6.3 is Galactic SNR.

Finally, we found a foreground open cluster that overlaps the SNR on the sky. It has an estimated age ~ 50 Myr and it is only ~ 140 pc away, with one B0 star (θ Carinae; see e.g. Fig. 1 in Nisak et al. 2022). This young cluster, which still has at least one star massive enough that it should explode as a core-collapse SN, could be home or somehow associated with G288.8–6.3 if it was closer. However, the surface brightness of G288.8–6.3 is so faint that it must be a physically large and middle-aged SNR, therefore cannot be this close to Earth. One could speculate that this object could be a wind bubble or some other type of wind-driven nebula, but we find this to be an unlikely scenario because there is not an obvious star near the centre that could be driving a wind.

4.3. H I Study of G288.8–6.3

In order to reveal the physical relation between the SNR and its surroundings, we analysed the archival H I data taken from HI4PI which has a modest angular resolution of 16' (HI4PI Collaboration et al. 2016). Figure 6(a) shows the velocity-integrated intensity map of H I towards the G288.8–6.3. We found a cavity-like distribution of H I in the velocity range from -2.5 to 9.1 km s⁻¹. The northeast and southern radio shell boundaries show a good spatial correspondence with H I clouds as shown in yellow to orange colour, suggesting the shock-cloud interaction occurred. On the other hand, the western radio shell with a blowout structure can be understood as the shocks travelling into the low-density space as shown in green to blue colour.

We also found other possible evidence for the shock-cloud interaction in p–v diagrams of H I. Figure 6(b) shows a hollowed distribution of H I in the V_{LSR} –Dec diagram, indicating the presence of an expanding H I shell formed by supernova shocks and/or strong winds from the progenitor. Although the R.A.– V_{LSR} diagram does not show such an expanding shell possibly due to the inhomogeneous gas distribution of H I, we found a high-velocity component within the radio shell (see the yellow box in Figure 6c). In SNRs, such a high-velocity component is thought to be formed by shock acceleration and provides an alternative support for the shock-cloud interaction (e.g., Koo et al. 1990).

Note that we also found another possible counterpart of H I with a different velocity range in terms of spatial

⁶ <http://www-wfau.roe.ac.uk/sss/halpha/hapixel.html>

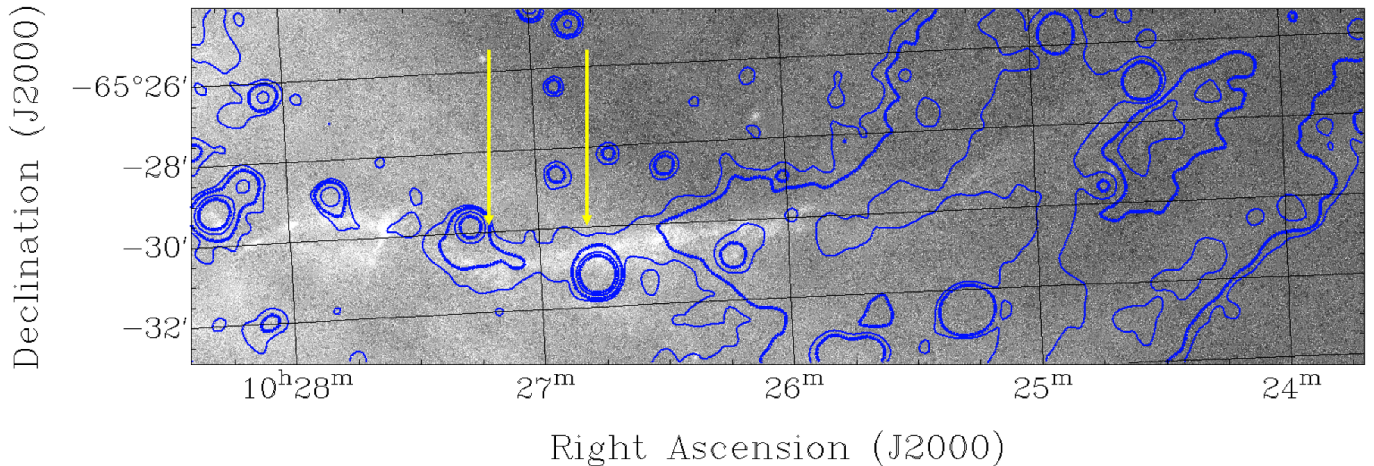


Figure 5. H α SuperCOSMOS grey scale (background subtracted) image overlaid with ASKAP contours (0.1, 0.2, 0.5 and 1 mJy beam⁻¹) of the Galactic SNR G288.8–6.3. Two yellow arrows indicate possible H α filament likely corresponding to radio emission. The area covering this image is marked in Figure 1 as the yellow rectangular box.

distributions of HI clouds and the radio shell which we could not rule out because of the modest angular resolution of the HI4PI data. Nonetheless, the kinematic distance to the SNR is expected to be small (few kpc) if the HI clouds at a velocity of ~ 0 km s⁻¹ are physically associated with the SNR. Further high-resolution HI observations are needed to test this possibility.

4.4. WISE view on SNR G288.8–6.3

We create a large 3 \times 3 degrees mosaic of the G288.8–6.3 SNR and its local environment as traced in the mid-infrared by the WISE bands of W1 (3.4 μ m), W2 (4.6 μ m), W3 (12 μ m) and W4 (23 μ m). The mosaics were created using the WISE WXSC pipeline (Jarrett et al. 2012) with native resolution (6'' in W1) and supersampled with 1'' pixels. As described in Jarrett et al. (2013, 2019), the WISE bands were uniquely designed to sample both stellar emission (W1 and W2), and Interstellar Medium (ISM) star-formation-excited gas/dust emission (W3 and W4). As expected, the stellar density is extremely high at these low Galactic latitudes, reaching the confusion limit of the WISE imaging resolution.

Inspection of bespoke WISE mid-infrared mosaics of the field did not yield any obvious spatial alignments with the radio continuum source. This rules out any strong dust or shock-excitation features emitted in the mid-infrared window (3–25 μ m) from the SNR candidate.

4.5. X-ray Observations and Data Analysis of G288.8–6.3

The X-ray data we report here were taken during the first five eROSITA all-sky surveys (Predehl et al. 2021; Sunyaev et al. 2021). G288.8–6.3 was mapped in a total of 210 telescope passages in the following date intervals:

January 8–16 and July 9–18, 2020; January 7–13 and July 15–21, 2021; January 12–18, 2022. The resulting averaged, vignetting corrected exposure time is 1607 s (~ 320 s per sky survey). The data we used in our analysis were processed by the eSASS (eROSITA Standard Analysis Software) pipeline (Brunner et al. 2022) and have the processing number #020. For the data analysis, we used eSASS version 211214 (released in December 21st 2021)⁷. Within the eSASS pipeline, X-ray data of the eRASS sky are divided into 4700 partly overlapping sky tiles of 3 $^{\circ}$.6 \times 3 $^{\circ}$.6 each. These are numbered using six digits, three for RA and three for Dec, representing the sky tile centre position in degrees. The majority of G288.8–6.3 falls into the eRASS sky tile numbered 156156, whereas the surrounding sky tiles 155153, 161153 and 163156 are required for complete coverage of G288.8–6.3.

Figure 7 depicts an RGB image of G288.8–6.3 which has been colour coded according to the energy of the detected X-ray photons. To produce the RGB image, we first created images for the three energy bands 0.2–0.7 keV, 0.7–1.2 keV, and 1.2–2.4 keV, respectively. eROSITA’s FOV averaged angular resolution during survey mode is 26''. The spatial binning in Figure 7 was set to 20'' in order to compensate for a small resolution reduction by the smoothing process. Data from all seven telescopes were used, as we did not notice a significant impact of the light leak in TM5 and TM7 (Predehl et al. 2021). In order to enhance the visibility of diffuse emission in the RGB image whilst leaving point sources unsmoothed to the greatest possible extent, we applied the adaptive kernel smoothing algo-

⁷ <https://erosita.mpe.mpg.de>

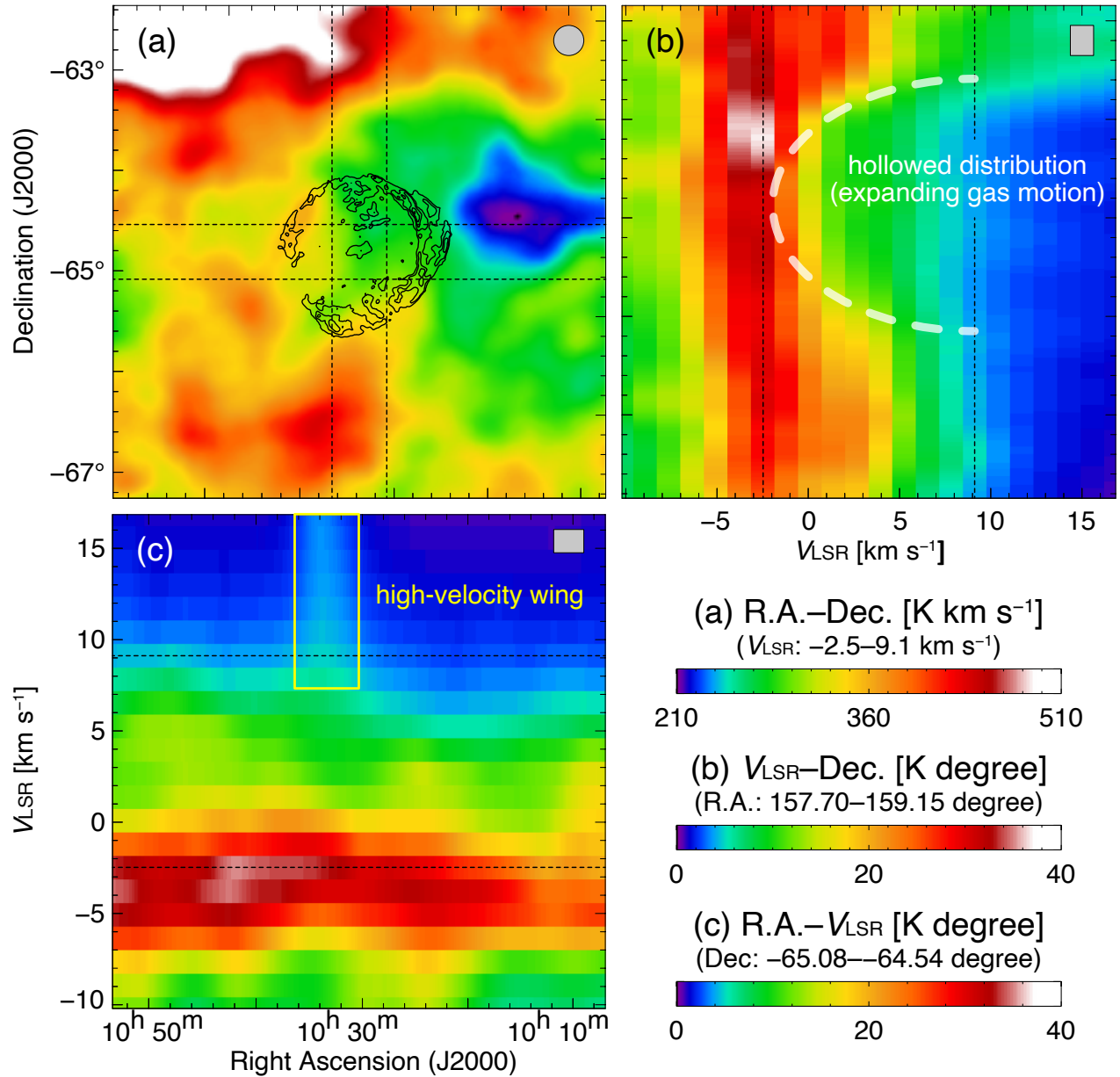


Figure 6. (a) Intensity distribution of HI obtained from HI4PI (HI4PI Collaboration et al. 2016). The integration velocity range is from -2.5 to 9.1 km s^{-1} . The superposed contours indicate the intensity of the radio continuum. (b)–(c) Position–velocity (p–v) diagrams of HI. The HI intensity is integrated from $157^{\circ}.70$ to $159^{\circ}.15$ in Right Ascension for (b) and from $-65^{\circ}.08$ to $-64^{\circ}.54$ in Declination for (c). The white dashed curve and yellow solid box in the p–v diagrams indicate candidates of an HI expanding shell and a high-velocity wing (see the text).

rhythm of Ebeling et al. (2006) with a Gaussian kernel of 3.0σ . As can be seen from Figure 7 there is faint diffuse X-ray emission filling the inner parts of G288.8–6.3 in the soft (0.2–0.7 keV) and medium (0.7–1.2 keV) energy band, partly overlapping with the radio contour lines of the remnant in the west and south-east. Whether this emission can be associated with G288.8–6.3 or whether it is part of an unrelated diffuse background structure is unclear. The low photon statistics do not allow us to perform a detailed spectral analysis.

4.6. Gamma-ray Observations of G288.8–6.3

SNRs are firmly established as gamma-ray emitters. Usually, bright gamma-ray emission is expected from SNRs in dense environments where pp-interactions create π_0 s that consequently decay into gamma-rays. Also, many bright TeV SNRs are quite young (less than a few kyr) and may have a significant inverse-Compton component from electrons. Older SNRs (beyond the synchrotron cooling time for electrons) however could have significant π^0 -decay components. However, the brightest known SNRs in TeV gamma-rays are all expanding into very low-density environments, similar to G288.8–6.3, where instead, high peak luminosities might be reached via inverse-Compton scattering (Brose et al. 2020).

The closest known gamma-ray source to G288.8–6.3 is 4FGL J1028.7–6431c from the Fermi-LAT catalogue of extended sources. 4FGL J1028.7–6431c is located $0^\circ.7$ away from the centre of G288.8–6.3 and hence roughly overlapping with the northern shell of the SNR (see Figure 1). The gamma-ray source has a detection significance of 5.6σ and the spectrum is described by a log parabola of the form

$$F(E) = F_0 \left(\frac{E}{E_0} \right)^{-\alpha - \beta \log(E/E_0)}, \quad (11)$$

with $F_0 = (1.5 \pm 0.3) \times 10^{-12} \text{ cm}^{-2} \text{ MeV}^{-1} \text{ s}^{-1}$, $\alpha = 2.6 \pm 0.3$ and $\beta = 0.4 \pm 0.2$ and a pivot energy of $E_0 = 720 \text{ MeV}$. The source is slightly elongated with a 68% containment radius of roughly 0.12° . Given that the gamma-ray emission is overlapping with a bright part of the radio shell, an association with G288.8–6.3 is likely but an association with PMN J1028–6441 was claimed earlier (Abdollahi et al. 2022).

The integrated photon flux of G288.8–6.3 is $F_{1-100\text{GeV}} = (2.6 \pm 0.6) \times 10^{-10} \text{ s}^{-1} \text{ cm}^2$. This is somewhat lower than the fluxes reported for other high-latitude extended Fermi sources such as FHES J1741.6–3917 ($(47.5 \pm 4.6) \times 10^{-10} \text{ s}^{-1} \text{ cm}^2$) and FHES J1208.7–5229 ($(9.6 \pm 1.6) \times 10^{-10} \text{ s}^{-1} \text{ cm}^2$) that are potentially associated with the well-evolved SNRs G351.0–5.4 and

G296.5+9.7 (Ackermann et al. 2018). However, given that the emission from 4FGL J1028.7–6431c is only originating from a part of the shell, emission from the rest of the remnant might be missed in the automated analysis. Further, Brose et al. (2021) showed that the emission morphology of evolved SNRs can extend well beyond the radio-emitting shell and becomes centre-filled for IC-dominated gamma-ray emitters due to the escape of accelerated particles. Hence, a dedicated analysis of Fermi-LAT data of the region is encouraged.

4.7. Evolutionary Status

To estimate the evolutionary status of this newly observed SNR, we apply the method presented in Urošević (2020, 2022). Using Pavlović et al. (2018) $\Sigma - D$ evolutionary tracks, we can conclude that G288.8–6.3 is an evolutionary advanced and low surface brightness SNR in the late Sedov or radiative phase of evolution (Figure 4). It evolves in a medium-density interstellar environment with densities $\sim 0.2 \text{ cm}^{-3}$. The energy of the SN explosion can be assumed to be the canonical 10^{51} erg . Additionally, G288.8–6.3's somewhat flatter spectral index ($\alpha = -0.41$) indicates possible Fermi 2 acceleration in addition to the DSA which can be characteristic of older SNRs (Onić 2013; Urošević 2014). The slight influence for appearing of flatter spectral indices in evolutionary evolved SNRs can be provided by the inclusion of thermal bremsstrahlung emission in addition to synchrotron emission, especially for SNRs that evolve in dense environments which is not the case for G288.8–6.3, but some fraction of the spectral index flattening can be explained by this kind of influence (Urošević et al. 2007; Onić et al. 2012). The next important issue for the determination of the evolutionary stage for G288.8–6.3 is from associated magnetic field values. In Section 2, we presented the derivation of the equipartition method for spectral index $\alpha > -0.5$ (adapted equipartition calculation). Both obtained values for the electron ($7.7 \mu\text{G}$, ambient field $2.3 \mu\text{G}$) and proton ($41.7 \mu\text{G}$, ambient field $12.6 \mu\text{G}$) equipartitions lead to the unique conclusion: shock-compression of the magnetic field (lower than a factor of 4) in this SNR is sufficient to produce large enough magnetic fields to explain the synchrotron emission of the SNRs. Further amplification of the magnetic field by the non-linear DSA effects is not required to explain the emission.

5. CONCLUSIONS

We discovered a nearby ($\sim 1.3 \text{ kpc}$), large angular size ($1^\circ.8 \times 1^\circ.6$) and low surface brightness galactic SNR G288.8–6.3 in the ASKAP-EMU survey. Its radio spectral index ($\alpha = -0.41 \pm 0.12$) is typical for an evo-

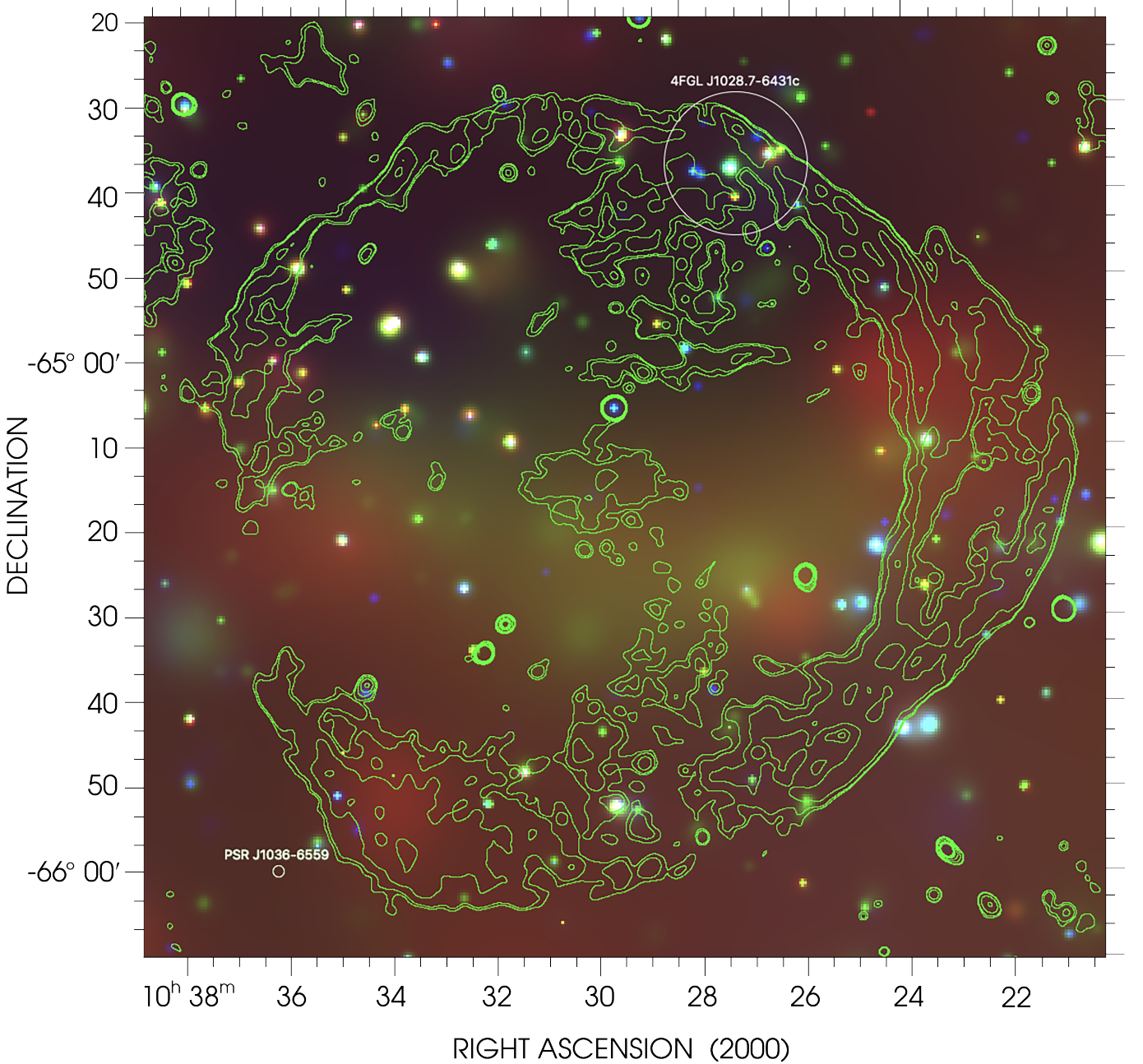


Figure 7. RGB image of G288.8–6.3 as seen in the eROSITA all-sky surveys eRASS:5. Photons to produce the image were colour coded according to their energy (red for energies 0.2–0.7 keV, green for 0.7–1.2 keV, blue for 1.2–2.4 keV). An adaptive kernel smoothing algorithm was applied to the images in each energy band. Radio contour lines (green: 0.1, 0.2, 0.5 and 1 mJy beam⁻¹) are overlaid to mark the outline of G288.8–6.3. The position of the neighbouring radio pulsar PSR J1036–6559, as well as of the Fermi source 4FG J1028.7–6431c, are shown.

lutionary advanced SNR population in the late adiabatic or in the radiative phases of evolution which evolves in a medium-density interstellar environment. We estimated its intrinsic size to be 40 pc, and its low radio surface brightness (at 1 GHz of $\Sigma = 1.4 \times 10^{-22} \text{ W m}^{-2} \text{ Hz}^{-1} \text{ sr}^{-1}$) suggests that it is about 13 000 years old. Based on the intrinsic size and the distance, it is located ~ 140 pc above the Galactic plane.

We derived equipartition formulae for determining G288.8–6.3 magnetic fields with spectral indices $\alpha > -0.5$ and estimated the magnetic field strength between $7.7 \mu\text{G}$ and $41.7 \mu\text{G}$ in the ambient field of $2.3 \mu\text{G}$ to $12.6 \mu\text{G}$, respectively.

From our HI study, we found a cavity-like distribution and possible evidence for the shock-cloud interaction. We detect some of the G288.8–6.3 filaments

in H α SuperCOSMOS survey and possible association with a gamma-ray source from the Fermi-LAT catalogue of extended sources – 4FGL J1028.7–6431c. WISE and eROSITA X-ray observations also point to some tantalising emissions that might be associated with G288.8–6.3.

Future in-depth polarimetric and multifrequency studies will enhance our knowledge of this large angular size Galactic object. Finally, given ASKAP’s sensitivity to low surface brightness emission, we anticipate many more similar discoveries as the EMU survey progresses.

6. ACKNOWLEDGMENTS

This scientific work uses data obtained from Inyarrimanha Ilgari Bundara / the Murchison Radio-astronomy Observatory. We acknowledge the Wajarri Yamaji People as the Traditional Owners and native title holders of the Observatory site. The Australian Commonwealth Scientific and Industrial Research Organisation (CSIRO)’s ASKAP radio telescope is part of the Australia Telescope National Facility⁸. Operation of ASKAP is funded by the Australian Government with support from the National Collaborative Research Infrastructure Strategy. ASKAP uses the resources of the Pawsey Supercomputing Research Centre. Establishment of ASKAP, Inyarrimanha Ilgari Bundara, the CSIRO Murchison Radio-astronomy Observatory and the Pawsey Supercomputing Research Centre are initiatives of the Australian Government, with support from the Government of Western Australia and the Science and Industry Endowment Fund. eROSITA is the soft X-ray instrument aboard SRG, a joint Russian-German science mission supported by the Russian Space Agency (Roskosmos), in the interests of the Russian Academy of Sciences represented by its Space Research Institute (IKI), and the Deutsches Zentrum für Luft- und Raumfahrt (DLR). The SRG spacecraft was built by Lavochkin Association (NPOL) and its subcontractors and is operated by NPOL with support from IKI and the Max Planck Institute for Extraterrestrial Physics (MPE). The development and construction of the eROSITA X-ray instrument was led by MPE, with contributions from the Dr. Karl Remeis Observatory Bamberg & ECAP (FAU Erlangen-Nürnberg),

the University of Hamburg Observatory, the Leibniz Institute for Astrophysics Potsdam (AIP), and the Institute for Astronomy and Astrophysics of the University of Tübingen, with the support of DLR and the Max Planck Society. The Argelander Institute for Astronomy of the University of Bonn and the Ludwig Maximilians Universität Munich also participated in the science preparation for eROSITA. The eROSITA data shown here were processed using the eSASS/NRTA software system developed by the German eROSITA consortium. MDF, GR and SL acknowledge Australian Research Council (ARC) funding through grant DP200100784. N.H.-W. is the recipient of ARC Future Fellowship project number FT190100231. SD is the recipient of an ARC Discovery Early Career Award (DE210101738) funded by the Australian Government. HS acknowledges funding from JSPS KAKENHI Grant Number 21H01136. DU and BA acknowledge the financial support provided by the Ministry of Science, Technological Development and Innovation of the Republic of Serbia through the contract 451-03-47/2023-01/200104, and for support through the joint project of the Serbian Academy of Sciences and Arts and Bulgarian Academy of Sciences on the detection of Galactic and extragalactic SNRs and HII regions. RB acknowledges funding from the Irish Research Council under the Government of Ireland Postdoctoral Fellowship program. JM acknowledges support from a Royal Society-Science Foundation Ireland University Research Fellowship (20/RS-URF-R/3712). CBS acknowledges support from a Royal Society Research Fellows Enhancement Award 2021 (22/RS-EA/3810). BV is funded by the Ministry of Education, Science and Technological Development of the Republic of Serbia through contract number 451-03-47/2023-01/200002. PJK acknowledges support from the Science Foundation Ireland/Irish Research Council Pathway programme under Grant Number 21/PATH-S/9360. We thank an anonymous referee for comments and suggestions that greatly improved our paper.

Facilities: ASKAP, MWA, Parkes, WISE, eROSITA, Fermi-LAT

Software: ASKAPsoft, AEGEAN (BANE)

REFERENCES

- Abdollahi, S., Acero, F., Baldini, L., et al. 2022, ApJS, 260, 53, doi: [10.3847/1538-4365/ac6751](https://doi.org/10.3847/1538-4365/ac6751)
- Ackermann, M., Ajello, M., Baldini, L., et al. 2018, ApJS, 237, 32, doi: [10.3847/1538-4365/aacdf7](https://doi.org/10.3847/1538-4365/aacdf7)
- Alsaberi, R. Z. E., Maitra, C., Filipović, M. D., et al. 2019, MNRAS, 486, 2507, doi: [10.1093/mnras/stz971](https://doi.org/10.1093/mnras/stz971)

⁸ <https://ror.org/05qajvd42>

- Araya, M., Hurley-Walker, N., & Quirós-Araya, S. 2022, *MNRAS*, 510, 2920, doi: [10.1093/mnras/stab3550](https://doi.org/10.1093/mnras/stab3550)
- Arbutina, B. 2017, *Publications de l'Observatoire Astronomique de Beograd*, 97, 1
- Arbutina, B., Urošević, D., Andjelić, M. M., Pavlović, M. Z., & Vukotić, B. 2012, *ApJ*, 746, 79, doi: [10.1088/0004-637X/746/1/79](https://doi.org/10.1088/0004-637X/746/1/79)
- Arbutina, B., Urošević, D., Vučetić, M. M., Pavlović, M. Z., & Vukotić, B. 2013, *ApJ*, 777, 31, doi: [10.1088/0004-637X/777/1/31](https://doi.org/10.1088/0004-637X/777/1/31)
- Arbutina, B., & Zeković, V. 2021, *Astroparticle Physics*, 127, 102546, doi: [10.1016/j.astropartphys.2020.102546](https://doi.org/10.1016/j.astropartphys.2020.102546)
- Arias, M., Botteon, A., Bassa, C. G., et al. 2022, *A&A*, 667, A71, doi: [10.1051/0004-6361/202244369](https://doi.org/10.1051/0004-6361/202244369)
- Ball, B. D., Kothes, R., Rosolowsky, E., et al. 2023, *MNRAS*, 524, 1396, doi: [10.1093/mnras/stad1953](https://doi.org/10.1093/mnras/stad1953)
- Bates, S. D., Bailes, M., Barsdell, B. R., et al. 2012, *MNRAS*, 427, 1052, doi: [10.1111/j.1365-2966.2012.22042.x](https://doi.org/10.1111/j.1365-2966.2012.22042.x)
- Becker, W., Hurley-Walker, N., Weinberger, C., et al. 2021, *A&A*, 648, A30, doi: [10.1051/0004-6361/202040156](https://doi.org/10.1051/0004-6361/202040156)
- Bell, A. R. 1978, *MNRAS*, 182, 147, doi: [10.1093/mnras/182.2.147](https://doi.org/10.1093/mnras/182.2.147)
- Blasi, P., Gabici, S., & Vannoni, G. 2005, *MNRAS*, 361, 907, doi: [10.1111/j.1365-2966.2005.09227.x](https://doi.org/10.1111/j.1365-2966.2005.09227.x)
- Bozzetto, L. M., Filipović, M. D., Vukotić, B., et al. 2017, *Astrophys. J. Suppl.*, 230, 2, doi: [10.3847/1538-4365/aa653c](https://doi.org/10.3847/1538-4365/aa653c)
- Bozzetto, L. M., Filipović, M. D., Sano, H., et al. 2023, *MNRAS*, 518, 2574, doi: [10.1093/mnras/stac2922](https://doi.org/10.1093/mnras/stac2922)
- Brose, R., Pohl, M., & Sushch, I. 2021, *A&A*, 654, A139, doi: [10.1051/0004-6361/202141194](https://doi.org/10.1051/0004-6361/202141194)
- Brose, R., Pohl, M., Sushch, I., Petruk, O., & Kuzyo, T. 2020, *A&A*, 634, A59, doi: [10.1051/0004-6361/201936567](https://doi.org/10.1051/0004-6361/201936567)
- Brunner, H., Liu, T., Lamer, G., et al. 2022, *A&A*, 661, A1, doi: [10.1051/0004-6361/202141266](https://doi.org/10.1051/0004-6361/202141266)
- Cajko, K. O., Crawford, E. J., & Filipovic, M. D. 2009, *Serbian Astronomical Journal*, 179, 55, doi: [10.2298/SAJ0979055C](https://doi.org/10.2298/SAJ0979055C)
- Calabretta, M. R., Staveley-Smith, L., & Barnes, D. G. 2014, *PASA*, 31, e007, doi: [10.1017/pasa.2013.36](https://doi.org/10.1017/pasa.2013.36)
- Camilo, F., Manchester, R. N., Gaensler, B. M., & Lorimer, D. R. 2002, *ApJL*, 579, L25, doi: [10.1086/344832](https://doi.org/10.1086/344832)
- Carretti, E., Haverkorn, M., Staveley-Smith, L., et al. 2019, *MNRAS*, 489, 2330, doi: [10.1093/mnras/stz806](https://doi.org/10.1093/mnras/stz806)
- Collischon, C., Sasaki, M., Mecke, K., Points, S. D., & Klatt, M. A. 2021, *A&A*, 653, A16, doi: [10.1051/0004-6361/202040153](https://doi.org/10.1051/0004-6361/202040153)
- Dokara, R., Brunthaler, A., Menten, K. M., et al. 2021, *A&A*, 651, A86, doi: [10.1051/0004-6361/202039873](https://doi.org/10.1051/0004-6361/202039873)
- Duncan, A. R., Stewart, R. T., Haynes, R. F., & Jones, K. L. 1997, *MNRAS*, 287, 722, doi: [10.1093/mnras/287.4.722](https://doi.org/10.1093/mnras/287.4.722)
- Ebeling, H., White, D. A., & Rangarajan, F. V. N. 2006, *MNRAS*, 368, 65, doi: [10.1111/j.1365-2966.2006.10135.x](https://doi.org/10.1111/j.1365-2966.2006.10135.x)
- Ferrand, G., & Safi-Harb, S. 2012, *Advances in Space Research*, 49, 1313, doi: [10.1016/j.asr.2012.02.004](https://doi.org/10.1016/j.asr.2012.02.004)
- Filipović, M. D., Payne, J. L., Jarrett, T., et al. 2021a, *European Journal of Science and Theology*, 17, 147, doi: [10.48550/arXiv.2103.13290](https://doi.org/10.48550/arXiv.2103.13290)
- Filipović, M. D., Ilić, M., Jarrett, T., et al. 2021b, *European Journal of Science and Theology*, 17, 11, doi: [10.48550/arXiv.2105.02119](https://doi.org/10.48550/arXiv.2105.02119)
- Filipović, M. D., Payne, J. L., Alsaberi, R. Z. E., et al. 2022a, *MNRAS*, 512, 265, doi: [10.1093/mnras/stac210](https://doi.org/10.1093/mnras/stac210)
- Filipović, M. D., Payne, J. L., Jarret, T., et al. 2022b, *European Journal of Science and Theology*, 18, 51, doi: [10.48550/arXiv.2206.00392](https://doi.org/10.48550/arXiv.2206.00392)
- Filipović, M. D., & Tothill, N. F. H., eds. 2021, *Multimessenger Astronomy in Practice*, 2514-3433 (IOP Publishing), doi: [10.1088/2514-3433/ac2256](https://doi.org/10.1088/2514-3433/ac2256)
- Finke, J. D., & Dermer, C. D. 2012, *ApJ*, 751, 65, doi: [10.1088/0004-637X/751/1/65](https://doi.org/10.1088/0004-637X/751/1/65)
- Foster, T. J., Cooper, B., Reich, W., Kothes, R., & West, J. 2013, *A&A*, 549, A107, doi: [10.1051/0004-6361/201220362](https://doi.org/10.1051/0004-6361/201220362)
- Gaensler, B. M., Landecker, T. L., Taylor, A. R., & POSSUM Collaboration. 2010, in *American Astronomical Society Meeting Abstracts*, Vol. 215, American Astronomical Society Meeting Abstracts #215, 470.13
- Galvin, T. J., & Filipovic, M. D. 2014, *Serbian Astronomical Journal*, 189, 15, doi: [10.2298/SAJ140505002G](https://doi.org/10.2298/SAJ140505002G)
- Gao, X. Y., Han, J. L., Reich, W., et al. 2011, *A&A*, 529, A159, doi: [10.1051/0004-6361/201016311](https://doi.org/10.1051/0004-6361/201016311)
- Ghavamian, P., Schwartz, S. J., Mitchell, J., Masters, A., & Laming, J. M. 2013, *SSRv*, 178, 633, doi: [10.1007/s11214-013-9999-0](https://doi.org/10.1007/s11214-013-9999-0)
- Green, D. A. 2022, *Cavendish Laboratory, Cambridge, United Kingdom* (available at "http://www.mrao.cam.ac.uk/surveys/snrs/")
- Guzman, J., Whiting, M., Voronkov, M., et al. 2019, *ASKAPsoft: ASKAP science data processor software*. <http://ascl.net/1912.003>
- Hancock, P. J., Murphy, T., Gaensler, B. M., Hopkins, A., & Curran, J. R. 2012, *MNRAS*, 422, 1812, doi: [10.1111/j.1365-2966.2012.20768.x](https://doi.org/10.1111/j.1365-2966.2012.20768.x)
- Hancock, P. J., Trott, C. M., & Hurley-Walker, N. 2018, *PASA*, 35, e011, doi: [10.1017/pasa.2018.3](https://doi.org/10.1017/pasa.2018.3)

- HI4PI Collaboration, Ben Bekhti, N., Flöer, L., et al. 2016, *A&A*, 594, A116, doi: [10.1051/0004-6361/201629178](https://doi.org/10.1051/0004-6361/201629178)
- Hotan, A. 2016, Holographic Measurement of ASKAP Primary Beams, Tech. Rep. ASKAP Commissioning and Early Science Memo 11, CSIRO Astronomy and Space Science. https://www.atnf.csiro.au/projects/askap/aces_memo011.pdf
- Hurley-Walker, N., Callingham, J. R., Hancock, P. J., et al. 2017, *MNRAS*, 464, 1146, doi: [10.1093/mnras/stw2337](https://doi.org/10.1093/mnras/stw2337)
- Hurley-Walker, N., Gaensler, B. M., Leahy, D. A., et al. 2019a, *PASA*, 36, e048, doi: [10.1017/pasa.2019.33](https://doi.org/10.1017/pasa.2019.33)
- Hurley-Walker, N., Filipović, M. D., Gaensler, B. M., et al. 2019b, *PASA*, 36, e045, doi: [10.1017/pasa.2019.34](https://doi.org/10.1017/pasa.2019.34)
- Ibrahim, A. Y., Borghese, A., Rea, N., et al. 2023, *ApJ*, 943, 20, doi: [10.3847/1538-4357/aca528](https://doi.org/10.3847/1538-4357/aca528)
- Jarrett, T. H., Cluver, M. E., Brown, M. J. L., et al. 2019, *ApJS*, 245, 25, doi: [10.3847/1538-4365/ab521a](https://doi.org/10.3847/1538-4365/ab521a)
- Jarrett, T. H., Masci, F., Tsai, C. W., et al. 2012, *AJ*, 144, 68, doi: [10.1088/0004-6256/144/2/68](https://doi.org/10.1088/0004-6256/144/2/68)
- . 2013, *AJ*, 145, 6, doi: [10.1088/0004-6256/145/1/6](https://doi.org/10.1088/0004-6256/145/1/6)
- Khabibullin, I. I., Churazov, E. M., Bykov, A. M., Chugai, N. N., & Sunyaev, R. A. 2023, *MNRAS*, 521, 5536, doi: [10.1093/mnras/stad818](https://doi.org/10.1093/mnras/stad818)
- Koo, B.-C., Reach, W. T., Heiles, C., Fesen, R. A., & Shull, J. M. 1990, *ApJ*, 364, 178, doi: [10.1086/169400](https://doi.org/10.1086/169400)
- Kothes, R., Reich, P., Foster, T. J., & Reich, W. 2017, *A&A*, 597, A116, doi: [10.1051/0004-6361/201629848](https://doi.org/10.1051/0004-6361/201629848)
- Luken, K. J., Filipović, M. D., Maxted, N. I., et al. 2020, *MNRAS*, 492, 2606, doi: [10.1093/mnras/stz3439](https://doi.org/10.1093/mnras/stz3439)
- Maggi, P., Filipović, M. D., Vukotić, B., et al. 2019, *Astron. & Astrophys.*, 631, A127, doi: [10.1051/0004-6361/201936583](https://doi.org/10.1051/0004-6361/201936583)
- Manchester, R. N., Hobbs, G. B., Teoh, A., & Hobbs, M. 2005, *AJ*, 129, 1993, doi: [10.1086/428488](https://doi.org/10.1086/428488)
- Misiriotis, A., Xilouris, E. M., Papamastorakis, J., Boumis, P., & Goudis, C. D. 2006, *A&A*, 459, 113, doi: [10.1051/0004-6361:20054618](https://doi.org/10.1051/0004-6361:20054618)
- Nisak, A. H., White, R. J., Yep, A., et al. 2022, *AJ*, 163, 278, doi: [10.3847/1538-3881/ac63c3](https://doi.org/10.3847/1538-3881/ac63c3)
- Norris, R. P., Marvil, J., Collier, J. D., et al. 2021, *PASA*, 38, e046, doi: [10.1017/pasa.2021.42](https://doi.org/10.1017/pasa.2021.42)
- Onić, D. 2013, *Ap&SS*, 346, 3, doi: [10.1007/s10509-013-1444-z](https://doi.org/10.1007/s10509-013-1444-z)
- Onić, D., Urošević, D., Arbutina, B., & Leahy, D. 2012, *ApJ*, 756, 61, doi: [10.1088/0004-637X/756/1/61](https://doi.org/10.1088/0004-637X/756/1/61)
- Pacholczyk, A. 1970, *Radio Astrophysics: Nonthermal Processes in Galactic and Extragalactic Sources*, *Astronomy and Astrophysics Series* (W. H. Freeman). <https://books.google.com.au/books?id=yQF-QgAACAAJ>
- Parker, Q. A., Phillipps, S., Pierce, M. J., et al. 2005, *MNRAS*, 362, 689, doi: [10.1111/j.1365-2966.2005.09350.x](https://doi.org/10.1111/j.1365-2966.2005.09350.x)
- Pavlović, M. Z., Urošević, D., Arbutina, B., et al. 2018, *Astrophys. J.*, 852, 84, doi: [10.3847/1538-4357/aaa1ef](https://doi.org/10.3847/1538-4357/aaa1ef)
- Predehl, P., Andritschke, R., Arefiev, V., et al. 2021, *A&A*, 647, A1, doi: [10.1051/0004-6361/202039313](https://doi.org/10.1051/0004-6361/202039313)
- Ranasinghe, S., & Leahy, D. 2022, *ApJ*, 940, 63, doi: [10.3847/1538-4357/ac940a](https://doi.org/10.3847/1538-4357/ac940a)
- Ranasinghe, S., Leahy, D., & Stil, J. 2021, *Universe*, 7, 338, doi: [10.3390/universe7090338](https://doi.org/10.3390/universe7090338)
- Reynolds, S. P., Gaensler, B. M., & Bocchino, F. 2012, *Space Science Reviews*, 166, 231, doi: [10.1007/s11214-011-9775-y](https://doi.org/10.1007/s11214-011-9775-y)
- Rudnick, L. 2002, *PASP*, 114, 427, doi: [10.1086/342499](https://doi.org/10.1086/342499)
- Stupar, M., Filipović, M. D., Parker, Q. A., et al. 2007, *Ap&SS*, 307, 423, doi: [10.1007/s10509-007-9394-y](https://doi.org/10.1007/s10509-007-9394-y)
- Stupar, M., Parker, Q. A., & Filipović, M. D. 2008, *MNRAS*, 390, 1037, doi: [10.1111/j.1365-2966.2008.13761.x](https://doi.org/10.1111/j.1365-2966.2008.13761.x)
- Sunyaev, R., Arefiev, V., Babyshkin, V., et al. 2021, *A&A*, 656, A132, doi: [10.1051/0004-6361/202141179](https://doi.org/10.1051/0004-6361/202141179)
- Taylor, A. R., Gibson, S. J., Peracaula, M., et al. 2003, *AJ*, 125, 3145, doi: [10.1086/375301](https://doi.org/10.1086/375301)
- Tingay, S. J., Goeke, R., Bowman, J. D., et al. 2013, *PASA*, 30, e007, doi: [10.1017/pasa.2012.007](https://doi.org/10.1017/pasa.2012.007)
- Urošević, D. 2014, *Ap&SS*, 354, 541, doi: [10.1007/s10509-014-2095-4](https://doi.org/10.1007/s10509-014-2095-4)
- . 2020, *Nature Astronomy*, 4, 910, doi: [10.1038/s41550-020-01228-5](https://doi.org/10.1038/s41550-020-01228-5)
- . 2022, *PASP*, 134, 061001, doi: [10.1088/1538-3873/ac6e4c](https://doi.org/10.1088/1538-3873/ac6e4c)
- Urošević, D., Pannuti, T. G., & Leahy, D. 2007, *ApJL*, 655, L41, doi: [10.1086/511780](https://doi.org/10.1086/511780)
- Urošević, D., Pavlović, M. Z., & Arbutina, B. 2018, *ApJ*, 855, 59, doi: [10.3847/1538-4357/aaac2d](https://doi.org/10.3847/1538-4357/aaac2d)
- Vukotić, B., Ćiprijanović, A., Vučetić, M. M., Onić, D., & Urošević, D. 2019, *Serbian Astronomical Journal*, 199, 23, doi: [10.2298/SAJ1999023V](https://doi.org/10.2298/SAJ1999023V)
- Wayth, R. B., Lenc, E., Bell, M. E., et al. 2015, *PASA*, 32, e025, doi: [10.1017/pasa.2015.26](https://doi.org/10.1017/pasa.2015.26)
- Wayth, R. B., Tingay, S. J., Trott, C. M., et al. 2018, *PASA*, 35, doi: [10.1017/pasa.2018.37](https://doi.org/10.1017/pasa.2018.37)
- Wolfire, M. G., McKee, C. F., Hollenbach, D., & Tielens, A. G. G. M. 2003, *ApJ*, 587, 278, doi: [10.1086/368016](https://doi.org/10.1086/368016)
- Wright, A. E., Griffith, M. R., Burke, B. F., & Ekers, R. D. 1994, *ApJS*, 91, 111, doi: [10.1086/191939](https://doi.org/10.1086/191939)
- Yao, J. M., Manchester, R. N., & Wang, N. 2017, *ApJ*, 835, 29, doi: [10.3847/1538-4357/835/1/29](https://doi.org/10.3847/1538-4357/835/1/29)
- Yew, M., Filipović, M. D., Stupar, M., et al. 2021, *MNRAS*, 500, 2336, doi: [10.1093/mnras/staa3382](https://doi.org/10.1093/mnras/staa3382)

Zhao, H., Jiang, B., Li, J., et al. 2020, ApJ, 891, 137,
doi: [10.3847/1538-4357/ab75ef](https://doi.org/10.3847/1538-4357/ab75ef)

Zirakashvili, V. N., & Aharonian, F. 2007, A&A, 465, 695,
doi: [10.1051/0004-6361:20066494](https://doi.org/10.1051/0004-6361:20066494)